Structural Isomerism in Crystals of Redox-Active Secondary *ortho*-Diamides: The Role of Competing Intra- and Intermolecular Hydrogen Bonds in Directing Crystalline Topologies

Stéphane A. Baudron,[a] Narcis Avarvari,[a] Enric Canadell,[b] Pascale Auban-Senzier,[c] and Patrick Batail*[a]

Abstract: The solid-state chemistry of a series of seven *ortho*-bis(alkylamido)-ethylenedithiotetrathiafulvalene derivatives EDT-TTF-$(CONHR)_2$ (R = Me, **1**; Et, **2**; Pr, **3**; Bu, **4**; Pent, **5**; Hex, **6**; and Bz, **7**), in their neutral and one-electron-oxidized, radical cation states, was investigated with an eye on the topology of intra- and intermolecular hydrogen-bond motifs. In the case of neutral, monomolecular solids, an intramolecular N−H···O hydrogen bond seals a constrained seven-membered ring for **1**, **2**, **3**, and **7**, which is disrupted in butyl derivative **4** in favor of an antiparallel ladder at the expense of any intramolecular hydrogen bond. In the solid-state, the competition between intra- and intermolecular hydrogen bonding observed in solution depends on the packing of the molecules. Electrocrystallization of methyl derivative **1** with ReO_4^- or ClO_4^-, two anions of different volumes but otherwise identical charge and symmetry, revealed a fine sensitivity of the constrained seven-membered ring to the internal chemical pressure exerted by the anion. $[\mathbf{1}]_2^{\cdot+}ReO_4$ ($\sigma_{RT} = 8.5\ S\,cm^{-1}$, activation energy $\Delta = 600$ K at high temperature) and β''-$[\mathbf{1}]_2^{\cdot+}ClO_4$ ($\sigma_{RT} = 0.03\ S\,cm^{-1}$, $\Delta = 1600$ K; under pressure at room temperature, the conductivity increases by three orders of magnitude up to 17 kbar with a linear variation of the activation energy with pressure, $\Delta = aP$ with $a = 0.202\ \ 10^6\ K\,kbar^{-1}$) have vastly different architectures, dimensionalities, electronic structures, and collective properties, a consequence of the presence of the closed or open structural isomers in one or the other. This exemplifies the flexibility of functionalized TTF derivatives, even when the functional group is directly attached to the electro-active core. This allows an analogy to be drawn with tetrafunctionalized metallocenes, in which such flexibility has already been observed. The experimental data are supported by theoretical calculations of the energy profile of a model molecule on rotation of the amido groups.

Keywords: amides · conducting materials · crystal engineering · hydrogen bonds · tetrathiafulvalene

Introduction

Hydrogen bonding,[1] the singular electrostatic, directing, and strongest of all intermolecular interactions[2] is one crystal engineers work with with confidence. N−H···O has been particularly studied because of its biological relevance, as it is observed to play a key role in proteins and enzymes.[3,4] Hence, amide functionality has been introduced into a variety of molecules, and their patterns of self-assembly in the solid state have been deciphered.[5] Likewise, seeking control over the dimensionality of intermolecular patterns of interactions[6] and a handle on a synergy with competing p_π–p_π intermolecular overlap interactions,[7,8] chemists working on tetrathiafulvalene (TTF)-based materials have prepared TTF derivatives bearing a thioamide,[9] an amide attached to the core directly[10] or through a spacer,[11] and uracil groups;[12] some of these were prepared as Langmuir–Blodgett films.[13] This strategy has been successful for the preparation of metallic materials.[7,14] However, in this field, only intermolecular hydrogen bonding has been considered as a tool for creating order in crystalline constructs. This is surprising, since intramolecular hydrogen bonding has been known for decades to influence the organization of pro-

[a] Dr. S. A. Baudron, Dr. N. Avarvari, Dr. P. Batail
Laboratoire Chimie, Ingénierie Moléculaire et Matériaux d'Angers
UMR 6200 CNRS-Université d'Angers
Bât. K, 2 Boulevard Lavoisier, 49045 Angers (France)
Fax: (+33) 241-735-011
E-mail: patrick.batail@univ-angers.fr

[b] Dr. E. Canadell
Institut de Ciència de Materials de Barcelona (CSIC)
Campus de la UAB, E-08193 Bellaterra (Spain)

[c] Dr. P. Auban-Senzier
Laboratoire de Physique des Solides
UMR 8502 CNRS-Université Paris-Sud
Bât. 510, 91405 Orsay (France)

  DOI: 10.1002/chem.200400153

teins,[3,4] was more recently shown to play a role in the solution and solid-state structures of calixarenes,[15] and the perspectives offered by modulating resonance-assisted N–H···O intramolecular hydrogen bonds have been convincingly advocated by Gilli et al.[16] and further advanced recently.[17,18] In order to address this point in TTF chemistry, we became interested in studying the materials chemistry of ethylenedithiotetrathiafulvalene functionalized with two secondary amido groups in *ortho* positions, EDT-TTF-$(CONHR)_2$. Owing to this particular arrangement, these two functional groups are susceptible to be positioned to form an intramolecular, hydrogen-bonded seven-membered ring. A recent CSD search showed that this kind of ring is much less probable than five- and six-membered rings,[19] mainly because it is constrained, especially when it contains an unsaturated bond (C=C). Hence, upon minute perturbations in the structure of the EDT-TTF-$(CONHR)_2$-based compounds, the intramolecular N–H···O hydrogen bond could vanish in favor of intermolecular network formation. Recent work along such lines has focused on the competition between inter- and intramolecular hydrogen bonding in the gas[20] and solution[21] phases. To probe the flexibility and fluxionality of TTF amide derivatives on lengthening the alkyl side chains, we report here on the synthesis and electrochemical and structural characterization of seven EDT-TTF-$(CONHR)_2$ (R = Me, **1**; Et, **2**; Pr, **3**; Bu, **4**; Pent, **5**; Hex, **6**, Bz, **7**) and demonstrate that on electrocrystallization[22] with two similar tetrahedral anions, namely ReO_4^- and ClO_4^-, the methyl derivative **1** yields two salts of identical stoichiometry with very different crystal structures. Hence, by contrast with the stubborn proclivity of the primary diamide EDT-TTF-$(CONH_2)_2$ to direct the assemblage of only one ribbon of self-complementary intra- and intermolecular amide···amide ring motifs, yet allowing for minute modulations of its curvature and shape,[23] the results presented here show that, among others, decoration with increasingly larger side chains sacrifices the conformational uniqueness of the intramolecular seven-membered ring. Furthermore, for R = Me, the occurrence of structural isomerism in radical cation salts is rooted in the fact that the hydrogen-bond ring conformer is open or closed, depending upon the nature of the anion. This strikes the balance between molecular shape, intermolecular connectivity, and electronic diversity examined in depth in this paper.

Results and Discussion

Synthesis of EDT-TTF-$(CONHR)_2$: EDT-TTF-$(CO_2Me)_2$[24] in CH_3CN reacts with NH_2R in aqueous solution at room temperature to afford after 24 h a precipitate of the corresponding EDT-TTF-$(CONHR)_2$, (R = Me, **1;** Et, **2**; Pr, **3**; Bu, **4**; Pent, **5**; Hex, **6** and Bz, **7**), which was filtered and recrystallized (Scheme 1). In contrast with the synthesis of the monoamide series EDT-TTF-$CONR^1R^2$,[10] this one-step reaction, described earlier by Bryce et al. for TTF itself,[25] does not require the preparation of the acid and carbonyl chloride derivatives. Note, however, that the reaction of the monoester with an excess of amine in aqueous solution does not yield the expected monofunctionalized amide EDT-TTF-CONHR. All EDT-TTF-$(CONHR)_2$ display two reversible oxidation waves (Table 1). As expected, attachment of a second amido group to the TTF core shifts the oxidation potential towards more anodic values, which are not sensitive to the length of the alkyl side chain. The oxidation potentials for EDT-TTF-$(CONHR)_2$ are only slightly higher (by 20 mV) than that of BEDT-TTF (BEDT-TTF = bis(ethylenedithio)tetrathiafulvalene).

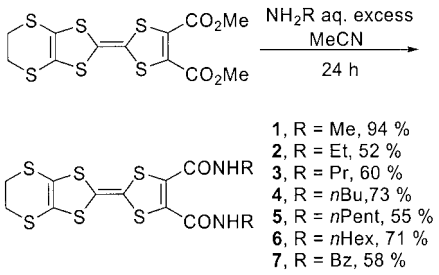

Scheme 1. Synthesis of **1**–**7**.

Table 1. Oxidation potentials of diamides **1**–**7** and some reference compounds (in V versus SCE, 0.05 M nBu_4NPF_6 in THF, 100 mV s^{-1}, 20 °C).

	$E^1_{1/2}$	$E^2_{1/2}$
EDT-TTF	0.59	0.83
BEDT-TTF	0.70	0.95
EDT-TTF-CONHMe	0.66	0.92
1–**7**	0.72	0.97

Structural isomerism in neutral one-component solids upon alkyl or aryl *N*-substitution: The crystal structures of **1**–**7**[26] were determined by single-crystal X-ray diffraction. Detailed crystallographic data are collected in Table 2. In their monomolecular, neutral crystalline forms, the methyl, ethyl, propyl and benzyl *N*-substituted derivatives all adopt the same closed configuration, exemplified for **1** in Figure 1, with a distinctive seven-membered ring motif clamped by a robust N–H···O hydrogen bond, whose characteristics are collected in Table 3.

In DMSO, $CDCl_3$, or CD_2Cl_2, the ^1H NMR spectra of **1**–**7** display a single peak for the two N–H groups, regardless of the functional group attached to the amide, an indication that, in solution, an equilibrium exists between the closed and open forms. Note that this seven-membered ring, which also includes a carbon–carbon double bond, is somewhat constrained,[19] and our attempts to detect a splitting of the single ^1H signal at temperatures as low as −90 °C in CD_2Cl_2 were unsuccessful. However, IR spectra of **1** and **4** in CH_2Cl_2 (10, 5, and 1 mM) reveal the presence of two bands. That at 3410–3420 cm^{-1} is attributed to free N–H, while that at 3260–3280 cm^{-1} corresponds to hydrogen-bonded N–H. Thus, the presence of intramolecular hydrogen bonding is ascertained in solution on the IR time scale.

Lengthening of the alkyl chain induces rotation of the carbonyl groups away from the mean plane of the constrained intramolecular seven-membered ring (Figure 2 and Table 4)

Table 2. Crystallographic data for **1**–**5** and **7**.

	1	**2**	**3**	**4**	**5**	**7**
formula	$C_{12}H_{12}N_2O_2S_6$	$C_{14}H_{16}N_2O_2S_6$	$C_{16}H_{20}N_2O_2S_6$	$C_{18}H_{24}N_2O_2S_6$	$C_{20}H_{28}N_2O_2S_6$	$C_{24}H_{20}N_2O_2S_6$
crystal size [mm]	0.09×0.09×0.60	0.06×0.06×0.62	0.21×0.23×0.48	0.06×0.12×0.54	0.08×0.12×0.62	0.02×0.08×0.62
T [K]	293 (2)	200 (2)	200 (2)	200 (2)	200 (2)	293 (2)
crystal system	monoclinic	monoclinic	monoclinic	triclinic	triclinic	monoclinic
space group	$P2_1/n$	$P2_1/n$	$P2_1/c$	$P\bar{1}$	$P\bar{1}$	$P2_1/n$
a [Å]	7.6289(10)	5.2793(4)	7.4518(5)	9.3702(13)	9.4142(15)	8.5697(8)
b [Å]	16.1235(10)	14.9705(16)	11.2160(12)	9.7971(14)	9.9683(16)	20.6744(14)
c [Å]	13.5175(10)	24.311(2)	24.6763(16)	13.9905(18)	14.573(2)	14.4027(12)
α [°]	–	–	–	109.230(15)	70.133(18)	–
β [°]	99.606(10)	95.143(8)	97.705(8)	106.623(16)	76.564(18)	90.671(10)
γ [°]	–	–	–	90.216(17)	89.890(19)	–
V [Å^3]	1639.4(3)	1913.7(3)	2043.8(3)	1155.2(3)	1246.5(4)	2551.6(4)
Z	4	4	4	2	2	4
ρ_{calcd} [g cm^{-3}]	1.656	1.516	1.510	1.417	1.388	1.460
μ [mm^{-1}]	0.840	0.725	0.684	0.609	0.569	0.562
reflections collected	3619	15683	15750	11840	12484	20283
independent reflections	3487	3620	3703	4200	4530	4950
R_{int}	0.035	0.052	0.081	0.050	0.065	0.098
observed reflections	2254	2119	2467	2468	2550	1489
parameters	199	217	235	253	256	307
R_1	0.0541	0.0331	0.0395	0.0333	0.0626	0.0303
wR_2	0.2164	0.0637	0.0987	0.0676	0.1783	0.0702
GOF	1.04	0.72	0.88	0.80	0.93	0.45
$\Delta\rho_{max/min}$ [e Å^{-3}]	0.60/−0.56	0.55/−0.31	0.54/−0.40	0.56/−0.28	0.97/−0.58	0.17/−0.14

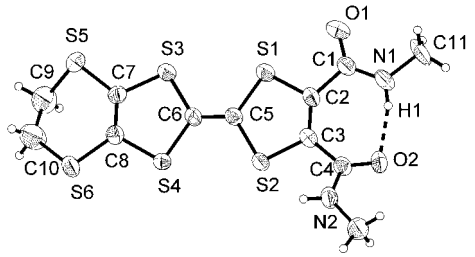

Figure 1. An ORTEP view of **1** in the crystal structure of its monocomponent solid, exemplifying the NH···O hydrogen bond and the intramolecular seven-membered ring (ellipsoids drawn at the 50% probability level).

Table 3. NH···O hydrogen-bond characteristics in **1**–**5** and **7**, and their comparison with CSD data.[51] α is the NH···O angle.

Cpd	Inter/Intra	Atom labeling	N···O [Å]	H···O [Å]	α [°]
1	Intra	N2–H2···O1	2.670 (6)	1.845	160.3
1	inter	N1–H1···O2	3.361 (6)	2.844	120.3
2	intra	N1–H1···O2	2.719 (3)	1.908	156.7
2	inter	N2–H2···O1	2.863 (3)	2.104	146.8
3	intra	N1–H1···O2	2.906 ()	2.089	158.5
3	inter	N2–H2···O1	2.944 ()	2.220	141.7
4	inter	N1–H1···O2	2.785 (3)	1.948	163.7
4	inter	N2–H2···O1	2.810 (3)	1.998	157.0
5	inter	N1–H1···O2	2.852(5)	2.009	164.2
5	inter	N2–H2···O1	2.839(5)	1.988	167.9
7	intra	N1–H1···O2	2.738 (4)	1.937	154.3
7	inter	N2–H2···O1	2.868 (4)	2.264	127.3
CSD	intra	–	2.755(12)	1.988(13)	132.5(15)
CSD	inter	–	2.892(3)	1.913(4)	161.2 (3)

up to angles for which the ring is disrupted for EDT-TTF-(CONH*n*Bu)$_2$ (**4**), EDT-TTF-(CONHPent)$_2$ (**5**), and EDT-TTF-(CONHHex)$_2$ (**6**)[26] in the solid state. These gradually evolving molecular conformations are expressed in the solid state by the evolving relative orientations of the remaining N–H and nearest-neighbor carbonyl oxygen atoms (Table 5). Hence, the diverse intermolecular N–H···O hydrogen bond motifs, ranging from isolated closed molecules for R = Me to antiparallel ladders built up of open molecules for R = *n*Bu, *n*Pent, *n*Hex, as detailed in Figures 3–5 and summarized in Figure 6.

Hollingsworth et al.[27] studied the effect of the lengthening of alkyl chains on the crystal structures of adducts of α,ω-dinitriles and urea, emphasizing the competition between packing efficiency and functional-group interactions. The simple 1:1 adducts formed for small chain lengths break into complex channel inclusion compounds for $n \geq 6$. In the present system, a discontinuity also appears, even though these are single-component solids. Here, the respective hydrogen-bond donor and acceptor character of N–H and C=O are satisfied in all structures, regardless of the open or closed molecular conformations. This implies that, in this competition, hydrogen bonding is always satisfied, a likely consequence of the variety of stable accessible networks (intramolecular seven-membered ring, extended chain motif, $R_4^4(16)$ ring,[28] antiparallel ladder, etc.). Moreover, even with a bulky group attached to the nitrogen atom, as in benzyl derivative **7**, the hydrogen-bond networks involve all available functionalities. This shows the synergistic effect of packing and hydrogen bonding, as suggested by Hagler and

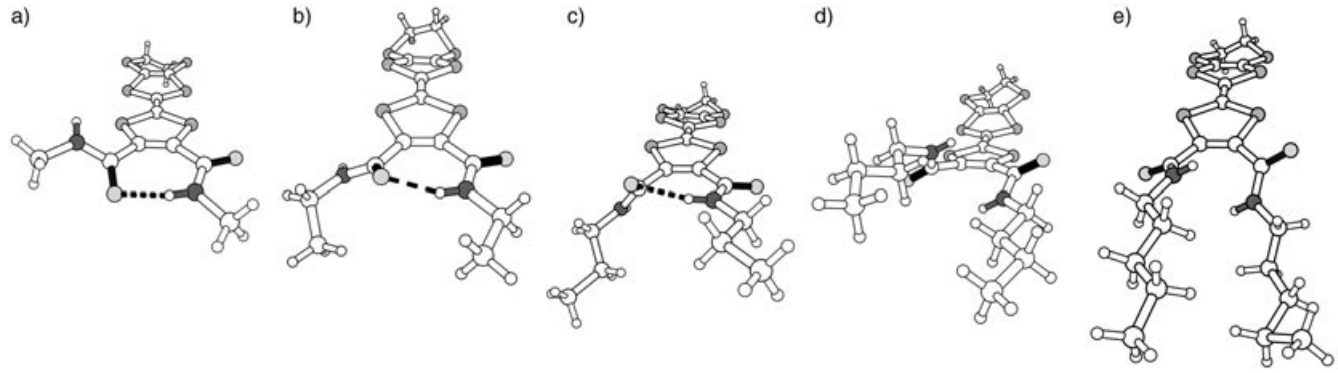

Figure 2. From closed to open molecular conformations (perspective views) on increasing the constraints imposed by bulkier *N*-alkyl substituents in the crystals of EDT-TTF-$(CONHR)_2$: a) R = Me; b) R = Et; c) R = Pr; d) R = *n*Bu; e) R = *n*Pent.

Table 4. Torsion angles of the amido groups with respect to the TTF core.

Cpd	N1-C1-C2-C3 [°]	C2-C3-C4-N2 [°]
1	4.9(9)	150.1(5)
2	6.2(5)	147.4(3)
3	16.6(5)	119.6(4)
4	41.7(5)	32.7(4)
5	36.2(7)	38.7(8)
7	20.6(6)	141.9(4)

Table 5. Intramolecular NH···S hydrogen-bond characteristics in **1**–**3** and **7**, and their comparison to CSD data for intramolecular NH···S hydrogen bonds in which S is divalent.[48]

Cpd	N···S [Å]	H···S [Å]	α [°]
1	2.929(4)	2.546	108.0
2	2.997(3)	2.648	105.7
3	3.117(4)	2.833	101.2
7	2.966(3)	2.547	111.1
CSD	3.12(2)	2.60(2)	113(1)

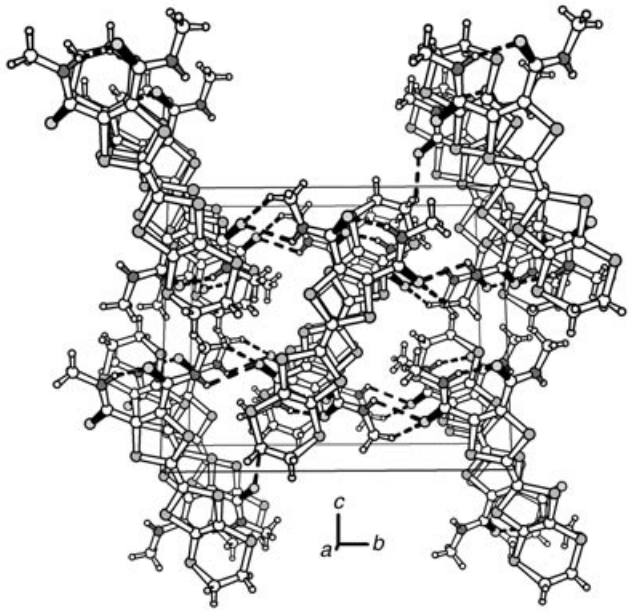

Figure 3. Perspective view of the unit cell of **1** down the *a* axis. Dashed lines represent intra- and intermolecular hydrogen bonds. Inversion-related dimers of EDT-TTF$(CONHMe)_2$ form slightly dimerized stacks (successive interplanar separations are 3.532(9) and 3.595(9) Å; see Figure 9a) which develop along *a*, an unusual feature for a flexible, neutral conjugated molecule in the solid state, for which classical herringbone-type arrangements are commonly observed. It has been suggested that one rare recent example of stacks of neutral molecules of fluorinated tetrathiafulvalenes was the consequence of fluorine segregation.[46] There is no such segregation here, but no strong hydrogen bond network is observed either, as the intermolecular NH/O=C interaction with neighboring molecules is very weak (see Figure 6a and Table 2). Note the respective *trans* configuration of all NH and C=O groups, which favors the appearance of a weak NH···S contact (Table 3), as observed earlier in the structure of $[Mo^{IV}O\{S_2C_2(CONH_2)_2\}_2]^{2-}$.[47] This kind of NH···S hydrogen bond has been shown to be especially weak when S is divalent,[48] as it is a very poor acceptor. Here intramolecular networks (seven-membered NH···O and five-membered NH···S rings) are clearly favored over competing intermolecular hydrogen bond motifs. Thus, increasing the number of hydrogen-bond donor and acceptor functionalities on the TTF core does not necessarily induce the formation of a strong intermolecular hydrogen-bond network.

Leiserowitz.[29] Indeed, among the several possible packing arrangements, the chosen one corresponds to a situation in which all donor and acceptor functionalities are satisfied.

The open and closed forms of these flexible, conjugated secondary *ortho*-diamides are in equilibrium in solution, as demonstrated by NMR experiments, and there is the possibility that the two forms could crystallize from solution as different polymorphs. However, the lattice energies of crystals of both forms are likely to be different enough to favor crystallization of a single form, in agreement with the absence of polymorphism. However, if we now consider crystalline assemblages of the one-electron-oxidized π donors with different anions, then, for a given donor, the two different structural isomers of one molecule could eventually be observed in the solid-state owing to different packing preferences. We now demonstrate how this assumption is verified by structural analysis of salts of the radical cation of EDT-TTF-$(CONHMe)_2$ (**1**) with ReO_4^- or ClO_4^-, two similar tetrahedral anions (Table 6). Remarkably, despite having the same stoichiometry, the two salts have vastly different architectures, dimensionalities, and electronic structures, a consequence of the presence of the closed or open structural isomers in one or the other.

Anion-dependent structural isomerism in two-component crystalline radical cation salts: In $[\mathbf{1}]_2^{\bullet+}ReO_4$, the radical cations are in the closed conformation (Figure 7) adopted in

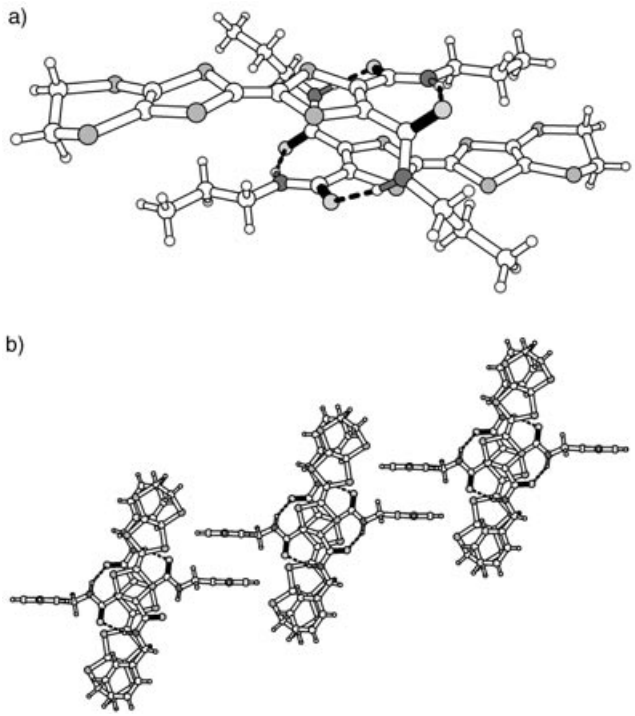

Figure 4. a) The bimolecular $R_4^4(16)$[28] hydrogen-bond motif which develops in the structure of **3** as a consequence of the partial rotation of the amido groups shown in Figure 2c. This cyclic motif induces the formation of hydrogen-bonded dimers that stack along the *a* axis. Note that the ordered $P2_1/c$ structure at 200 K is displayed here. In the room-temperature $P2_1/n$ structure, the unit cell contains two molecules with severely disordered propyl groups. A phase transition was detected at 258 K by differential scanning calorimetry and was confirmed by single-crystal X-ray diffraction. Below the transition, the *a* axis becomes twice as small, and the single molecule in the unit cell is ordered. b) A similar bimolecular $R_4^4(16)$ hydrogen-bond motif observed in the structure of **7**.

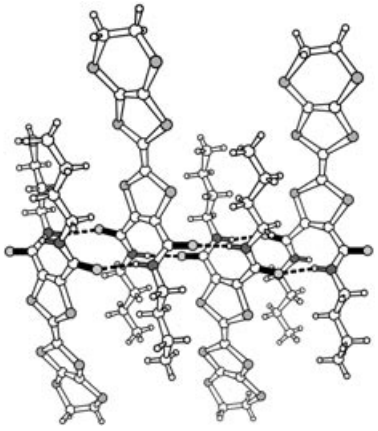

Figure 5. Perspective view of the infinite antiparallel ladder motif in the structure of **4**, which develops as a consequence of its open conformation, shown in Figure 2d. Antiparallel ladders are a common feature of secondary diamides.[49] The molecules in the ladder are related by an inversion center. As a consequence, there are no short S···S contacts within the ladder.

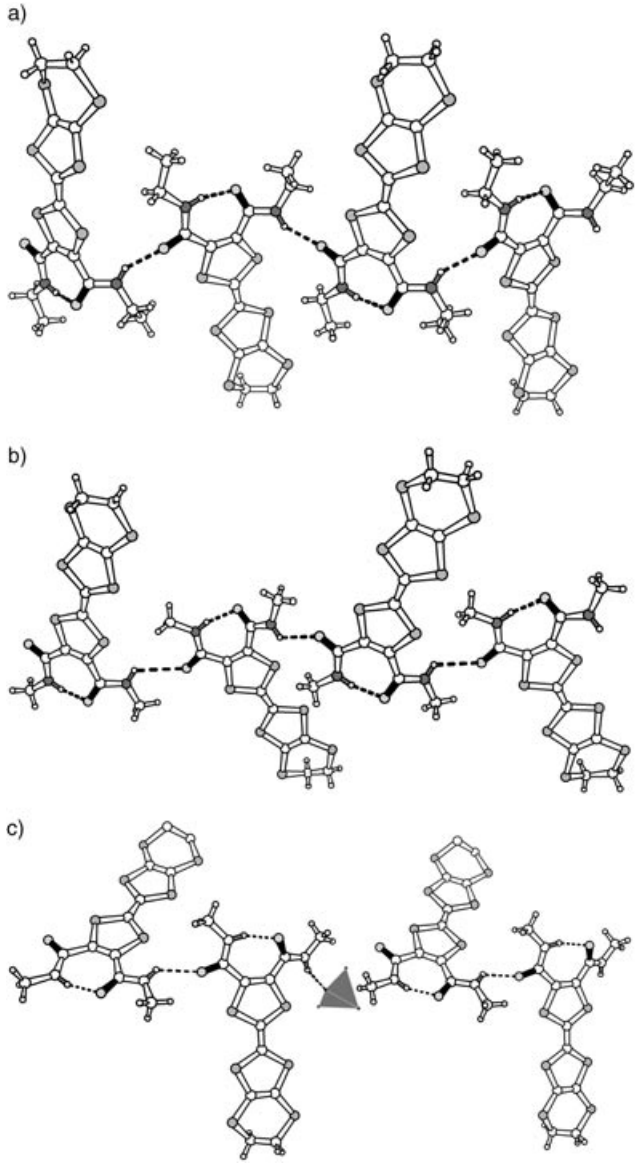

Figure 6. A set of representations (perspective views) exemplifying the common infinite-chain motif which develops through NH···O hydrogen bonds in the structures of a) EDT-TTF-$(CONHEt)_2$; b) EDT-TTF-$(CONHMe)_2$; and its relationship with c) the broken sequence in $[\mathbf{1}]_2^{\cdot+}ReO_4$. This type of chain was observed previously in the structures of a number of secondary amides.[50] It is also present in the structure of the neutral monofunctionalized EDT-TTF-CONHMe.[10]

the structure of the neutral form (Figures 1–3 and 6). The two independent molecules A and B stack along *a* to form two well-separated columns (Figure 7), and the single anion is disordered. The infinite chain motif present in the monocomponent solid EDT-TTF-$(CONHMe)_2$ (Figure 6a) is not stabilized in $[EDT\text{-}TTF\text{-}(CONHMe)_2]_2ReO_4$ (Figure 6c). Instead, one oxygen atom of ReO_4^- competes favorably with carbonyl oxygen atoms of the neighboring molecules for the single available N–H hydrogen-bond donor. This results in the broken sequence shown in Figure 6c. This is a novel manifestation of the synergy of the weaker hydrogen-bond acceptor character of the amide carbonyl oxygen atom in such oxidized radical cations.[17]

The calculated band structure for the three-dimensional donor network of $[\mathbf{1}]_2^{\cdot+}ReO_4$ at 298 K is shown in Figure 8. Calculations on the crystal structure at 150 K led to almost identical results, except for a slight increase in the band dis-

Table 6. Crystallographic data for $[\mathbf{1}]_2^{\cdot+}ReO_4$ and $[\mathbf{1}]_2^{\cdot+}ClO_4$.

	$[\mathbf{1}]_2^{\cdot+}ReO_4$	$[\mathbf{1}]_2^{\cdot+}ReO_4$	$[\mathbf{1}]_2^{\cdot+}ClO_4$
formula	$C_{24}H_{24}N_4O_6S_{12}Re$	$C_{24}H_{24}N_4O_6S_{12}Re$	$C_{24}H_{24}N_4O_6S_{12}Cl$
crystal size [mm]	0.06×0.06×0.62	0.06×0.06×0.62	0.15×0.30×0.60
T [K]	293 (2)	150 (2)	293 (2)
crystal system	triclinic	triclinic	triclinic
space group	$P\bar{1}$	$P\bar{1}$	$P\bar{1}$
a [Å]	7.6968(6)	7.6222(9)	9.2949(10)
b [Å]	14.1003(11)	14.0862(16)	11.3568(10)
c [Å]	18.0346(13)	17.953(2)	17.4397(10)
α [°]	68.247(9)	68.626(12)	95.907(10)
β [°]	79.092(9)	78.327(13)	91.803(10)
γ [°]	80.121(9)	79.662(13)	100.124(10)
V [Å^3]	1773.9(3)	1746.0(4)	1800.3(3)
Z	2	2	2
ρ_{calcd} [g cm^{-3}]	2.023	2.023	1.691
μ [mm^{-1}]	4.251	4.251	0.854
reflections collected	17205	17503	8248
absorption correction	numerical	numerical	psi scan
T_{min}/T_{max}	0.6943/0.8592	0.7023/0.8592	0.582/0.651
independent reflections	6363	6317	7028
R_{int}	0.055	0.052	0.016
observed reflections	3874	4998	4750
parameters	442	442	443
R_1	0.0386	0.0232	0.0461
wR_2	0.0711	0.0489	0.1482
GOF	0.81	0.88	1.08
$\Delta\rho_{max/min}$ [e^{-3} Å]	2.47/−1.51	0.70/−0.93	0.91/−0.51

persion. The donor network contains two different types of columns with donors having the long molecular axis parallel (A) or tilted (B) with respect to the *b* axis (see Figure 7). From a purely structural viewpoint the stacks of donor A are quite uniform (Figure 9b), with a bond-over-ring type of overlap, whereas those of donor B are built up of eclipsed dimeric units (Figure 9c). As shown in Figure 8 the band dispersion along the Γ→Y and Γ→Z directions is nil, so that the system can be described as a series of noninteracting chains. Thus the bands in Figure 8 can be associated with a specific type of chain (bands a_1/a_2 and b_1/b_2 with the chains of donors A and B, respectively). Note that crossing between bands b_2 and a_2 along $\Gamma\rightarrow X$ is avoided. Bands b_1 and b_2 are strongly separated in energy, as suggested by the dimerization noted in that chain. In contrast, the topology of bands a_1 and a_2 is typical for a quite uniform chain with only minute structural dimerization (i.e., leading to the dimerization gap at X). Because of the stoichiometry, the four bands of Figure 8 must contain two holes. Thus, this band structure would suggest that $[\mathbf{1}]_2^{\cdot+}ReO_4$ must be a band-gap semiconductor and thus diamagnetic. However, this description implicates that donors A are neutral, whereas donors B have a positive charge, something which does not quite harmonize with the small difference in the central C=C bond lengths of the two donors (1.353 and 1.368 Å for donors A and B, respectively), which in addition are both slightly longer than the central C=C bond in **1** (1.335(8) Å). This suggests that electron repulsions may split each of the a_1 and b_1 bands into two Mott–Hubbard subbands in such a way that one of the two a_1/b_1 subbands is filled and the other is empty. This leads to an alternative description of this salt as containing two different chains bearing unpaired electrons (Figure 9). These chains are different from both the structural and electronic viewpoints: although the building block is a $[EDT\text{-}TTF(CONHMe)_2]_2^+$ unit in both cases, the chains are either strongly dimerized or quite uniform in the case of donors B and A, respectively. Detailed physical tests are needed to distinguish among the two alternative descriptions.

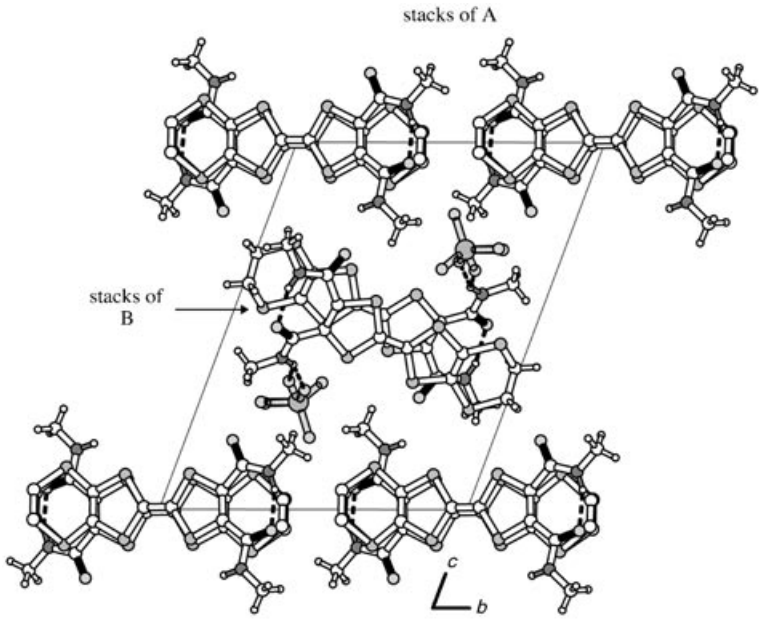

Figure 7. Projection down the *a* axis of the crystal structure at 150 K of $[\mathbf{1}]_2^{\cdot+}ReO_4$. Molecules A and B segregate into two different stacks. Molecules A are slipped (bond-over-ring pattern) with respect to their long axis, and molecules B are both slipped and offset along their transverse, short axis.

The structure of TTF-based materials is typically not affected on substitution of ClO_4^- for ReO_4^-. Here, however, $[\mathbf{1}]_2^{\cdot+}ClO_4$ is not isostructural to $[\mathbf{1}]_2^{\cdot+}ReO_4$. Again, there are two independent π-donor mole-

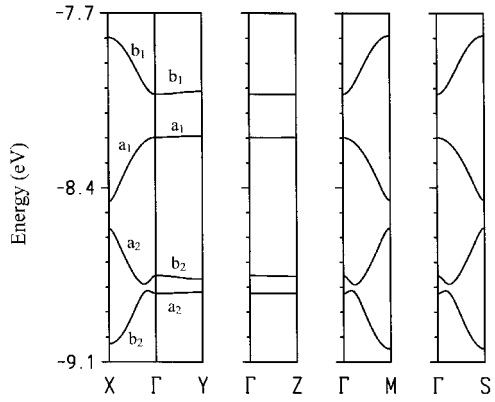

Figure 8. Calculated band structure for the donor network of $[\mathbf{1}]_2^{\cdot+}ReO_4$ at 298 K. Γ = (0, 0, 0), X = (a*/2, 0, 0), Y = (0, b*/2, 0), Z = (0, 0, c*/2), M = (a*/2, b*/2, 0), and S = (−a*/2, b*/2, 0).

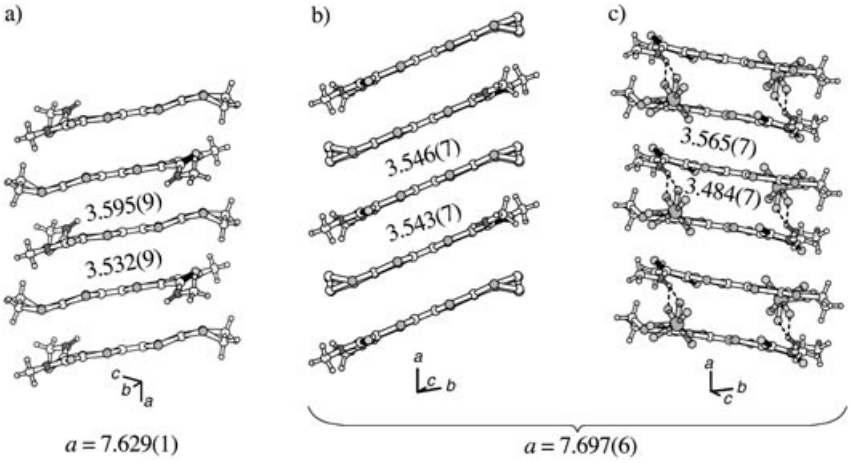

Figure 9. a) Topology of the slipped and only slightly dimerized stacks of neutral molecules in EDT-TTF-$(CONHMe)_2$; b) the strikingly similar A-stack topology; and c) the dimerized B-stack topology in $[\mathbf{1}]_2^{\cdot+}ReO_4$. The intrastack intermolecular distances and stacking axis parameters a [Å] are indicated.

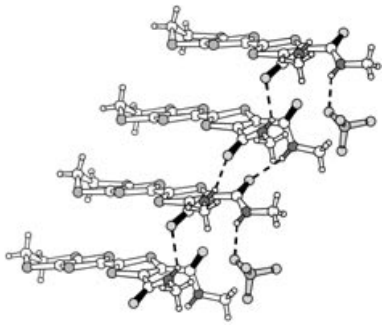

Figure 10. The association of an infinite chain motif and an anion-interrupted sequence (shown in perspective) in the hydrogen-bonded interfacial backbone in β″-$[\mathbf{1}]_2^{\cdot+}ClO_4$ (only one of the two disordered positions of the anion is represented), also exemplifying the open conformation of this structural isomer, which differs from the closed form adopted in the structure of **1** (Figure 2a). Remarkably, although the volume of ClO_4^- is about 30% smaller than that of ReO_4^-,[32] the unit-cell volume of β″-$[\mathbf{1}]_2^{\cdot+}ClO_4$ is slightly larger (by 1.4%, Table 5) than that of $[\mathbf{1}]_2^{\cdot+}ReO_4$, in which a stronger chemical pressure is exerted on the molecules in the solid. In addition, note that the density of β″-$[\mathbf{1}]_2^{\cdot+}ClO_4$ is about 6% lower than that of $[EDT\text{-}TTF\text{-}(CONH_2)_2]_2ClO_4$.[23] One therefore expects the lattice of the present ClO_4^- salt to be rather soft, certainly softer than that of the ReO_4^- salt, and especially sensitive to external isotropic pressure, as is indeed exemplified by Figures 14 and 15.

cules and one disordered anion in the unit cell at room temperature. Both independent molecules are now in the open conformation (Figure 10) observed earlier for R = nBu, nPent, nHex (Figure 2d). Note also the pattern of intermolecular overlap between the radical cations (Figure 11), now arranged in slabs of the β″ type.[30] Absence of polymorphism was ascertained by visual inspection of the crystal morphologies ($[\mathbf{1}]_2^{\cdot+}ReO_4$ crystallizes as long needles while β″-$[\mathbf{1}]_2^{\cdot+}ClO_4$ crystallizes as long rods) and X-ray powder diffraction. Since the single-crystal structures of $[\mathbf{1}]_2^{\cdot+}ReO_4$ and β″-$[\mathbf{1}]_2^{\cdot+}ClO_4$ proved to be different, X-ray powder diagrams of the compounds were collected on batches obtained by accumulating crystals from several electrocrystallization experiments. Remarkably, as exemplified in Figure S1 (Supporting Information), the diagrams are identical to those simulated from the respective single-crystal data, which ascertain the absence of polymorphism in the series. Thus, a seemingly minor change, that is, replacing ClO_4^- by ReO_4^- in the electrocrystallization experiment, while keeping the same conditions of current density, temperature, solvent, and concentration, results in selective stabilization of the planar, closed conformer instead of the perpendicular, open conformer, a change of conformation and molecular shape which ultimately transforms the structural organization of their radical cation salts. Because of the open molecular conformation, there are two pairs of NH and C=O functionalities available for intermolecular hydrogen bonding. Therefore, the interfacial organic–inorganic pattern of interactions (Figure 10) in β″-$[\mathbf{1}]_2^{\cdot+}ClO_4$ is the simple coassociation of the infinite N−H···O chain motif correlating

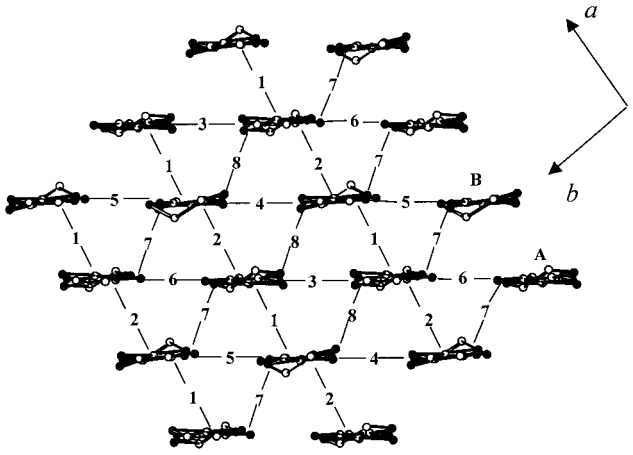

Figure 11. The β″ donor layer in $[\mathbf{1}]_2^{\cdot+}ClO_4$ with labeling of the different types of interactions and donors.

the closed conformers in neutral EDT-TTF-$(CONHMe)_2$ (Figure 6a) and EDT-TTF-$(CONHEt)_2$ (Figure 6b) with the shortened sequences, interrupted by NH···$OClO_3^-$ hydrogen bonds, as observed in $[EDT\text{-}TTF\text{-}(CONHMe)_2]_2ReO_4$ (Figure 6c).

The β″ donor layer contains two different donors (labeled A and B in Figure 11) and eight different donor···donor interactions (labeled 1–8 in Figure 11). The central C=C bond lengths for the two donors are 1.342 and 1.379 Å for A and B, respectively, and the corresponding HOMO energies are −8.678 and −8.402 eV. These observations together with the stoichiometry suggest that donors A could be considered as neutral, whereas donors B should bear a positive charge. Surprisingly, the calculated band structure (see Figure 12a) contains four HOMO bands with dispersions not far from those of the usual metallic β″ BEDT-TTF salts,[31] and this suggests considerable delocalization. The two upper bands overlap, and since the stoichiometry indicates that these bands should contain two holes, both types of bands must be partially filled, which leads to the Fermi surface of Figure 12b. This Fermi surface formally contains three types of closed contributions: two different hole pockets centered at X and Y and an electron pocket centered at M. However, as schematically shown in Figure 12b, this Fermi surface can be described as resulting from the hybridization of a series of superposed ellipses, as usually observed for β″ phases.[31]

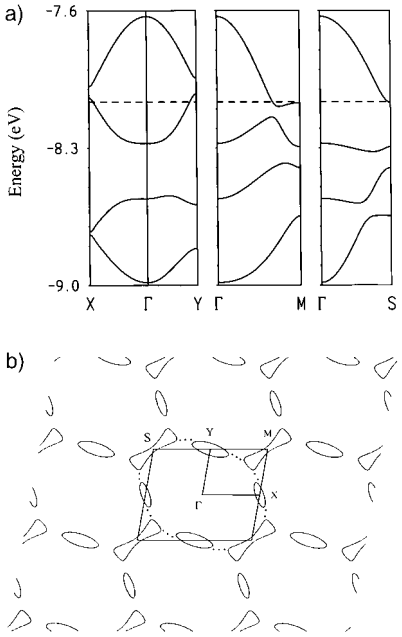

Figure 12. Calculated band structure (a) and Fermi surface (FS); b) for the donor layers of β″-$[\mathbf{1}]_2^{\cdot+}ClO_4$. The description of the FS as resulting from the hybridization of a series of superposed ellipses is schematically indicated by dots in b). The dashed line in a) refers to the Fermi level for the assumption of metallic filling of the bands. Γ = (0, 0), X = (a*/2, 0), Y = (0, b*/2), M = (a*/2, b*/2), and S = (−a*/2, b*/2).

A careful analysis of the upper pair of band wavefunctions for different points of the Brillouin zone clearly shows that the band dispersion results from strong mixing of the HOMOs of the two types of donors, even though those of B have a stronger contribution. The reason for this are the very favorable HOMO···HOMO intermolecular overlaps along the inclined π stacks in the a direction and the step-chains along the b direction, that is, the two directions for which the intermolecular interactions are of the A···B type. The difference in HOMO energies between the two donors effectively reduces the magnitude of the transfer integrals along these directions. In this way, these transfer integrals become very similar to those along the chains of identical molecules (A···A··· and B···B···) making lateral contacts (and thus weaker π-type overlaps) along the $a+b$ direction. These interactions are very similar in magnitude to those occurring in the usual BEDT-TTF β″ salts. The result is an effective, very uniform, and far from negligible set of interactions between the HOMOs, which leads to the band structure of Figure 12a. Consequently, this analysis suggests that in the absence of disorder the salt should be metallic, but activated electrical conductivity is observed instead (Figure 13). The disorder experienced on the anion site must be responsible for the "abnormal" activated conductivity. It is thus quite likely that the metallic state could be stabilized under pressure.

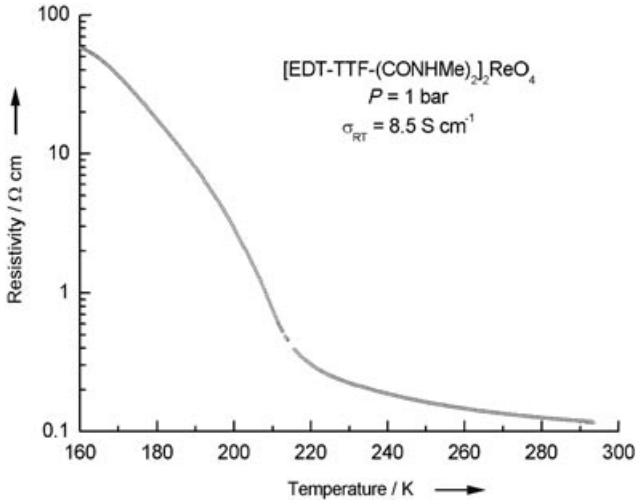

Figure 13. Temperature dependence of the resistivity at ambient pressure for $[\mathbf{1}]_2^{\cdot+}ReO_4$

Activated conductivity: Despite the sizeable conductivity at room temperature ($\sigma_{RT} = 8.5\ S\,cm^{-1}$), the resistivity at ambient pressure of $[\mathbf{1}]_2^{\cdot+}ReO_4$ exhibits an activated temperature dependence [$\rho = \rho_0 \exp(\Delta/T)$] with an activation energy of $\Delta = 600$ K at high temperature (Figure 13). Note that the change in slope observed at 212 K is not associated with a structural phase transition, since the crystal structures determined at 293 K and 150 K are identical.

The room-temperature conductivity of β″-$[\mathbf{1}]_2^{\cdot+}ClO_4$ is lower ($\sigma_{RT} = 0.03\ S\,cm^{-1}$) with a pronounced activated temperature dependence ($\Delta = 1600$ K). However, under pressure at room temperature, the conductivity increases rapidly (by more than three orders of magnitude up to 17 kbar), with an exponential variation up to 8 kbar then a linear variation (Figure 14). This exponential dependence in an insu-

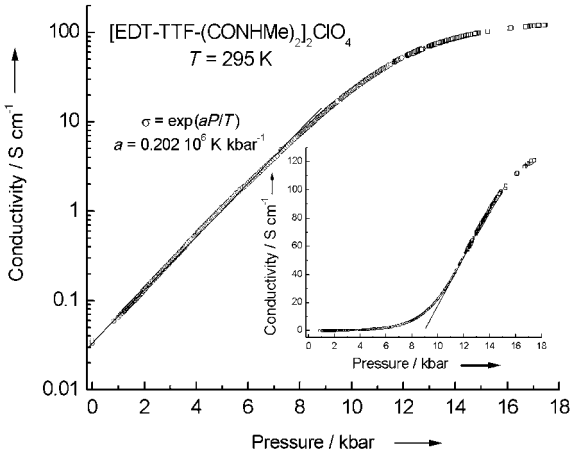

Figure 14. Pressure dependence of the conductivity (logarithmic scale) at room temperature for β″-[**1**]$_2$·$^+$ClO$_4$; inset: the same data plotted with a linear scale for the conductivity.

lating regime could be attributed to a linear variation of the activation energy with pressure, $\Delta = aP$ with $a = 0.202 \times 10^6$ K kbar^{-1}. In the range of 10–15 kbar, $\sigma(P)$ shows a linear behavior similar to that of TMTTF and TMTSF salts (TM = transition metal) but with a steeper slope (insert of Figure 14). This strong linear variation of the activation energy with pressure is consistent with a particularly soft lattice for β″-[**1**]$_2$·$^+$ClO$_4$, as discussed below and in Figure 10. The temperature dependencies of the resistivity at 12.3 and 16.7 kbar, depicted on Figure 15, remain activated, with activation energies decreasing with pressure, despite the small values of the resistivities at room temperature (17 and 8.7 mΩ cm, respectively). However, below 160 and 220 K, respectively, for these two pressures, a strong increase in the activation energy takes place, perhaps related to a structural transition which may involve a change of topology of the molecule, back to the closed isomer conformation, as discussed below.

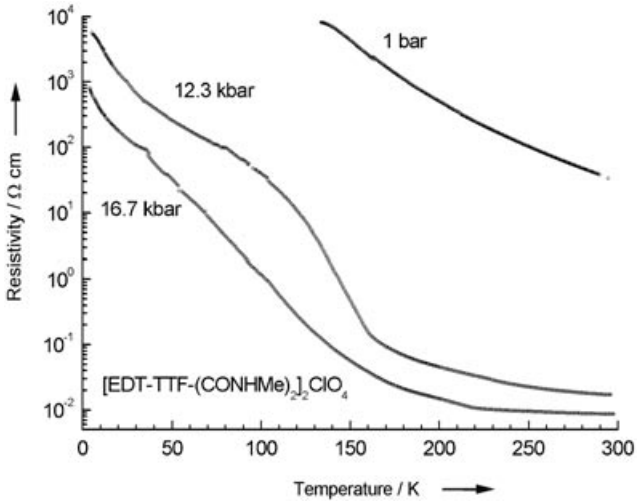

Figure 15. Temperature dependence of the resistivity at 1 bar, 12.3 kbar, and 16.7 kbar for β″-[**1**]$_2$·$^+$ClO$_4$.

Comments on the flexibility of the molecular shape and network topology, an expression of the stereodynamics of bond rotation: The stabilization in the solid state of one or the other conformer results in two different crystal structures with different patterns of N–H···O intermolecular associations. Remarkably, by association with any one of these two anions only one conformer is stabilized and one crystal structure constructed. Among the many experiments conducted, no evidence was found for crossed-structure stabilization. In other words, in no instance have the two different crystal structures been obtained with either ReO_4^- or ClO_4^-. As the volume of the latter is about 30 % smaller,[32] this unprecedented outcome may indicate a fine sensitivity of the constrained intramolecular seven-membered ring to a decreased chemical pressure exerted on the molecules in the lattice by engaging a smaller anion, as commented further in the caption to Figure 10. Note, however, that in both cases the anions act essentially the same by accepting one N–H hydrogen-bond donor. This is considered significant given that monoamide-functionalized EDT-TTFs have been shown to express the O_h and T_d anion symmetries of AsF_6^- and ReO_4^- in the different stoichiometries and crystal structures of [EDT-TTF-CONH$_2$]$_6$AsF$_6$ and [EDT-TTF-CONH$_2$]$_2$ReO$_4$, respectively.[7] Thus, it is the synergy between the topologies of the two major stereodynamic conformers in the solution, defined as an inherent molecular flexibility, which is expressed at the large length scales of a macroscopic single crystal by virtue of different cooperative hydrogen-bond networks. Direct attachment of a functional group to the TTF core has been regarded so far as a source of cooperativity between the recognition pattern directed by this functionality and the p_π–p_π overlap of the TTF cores. Indeed, introduction of a spacer between the functional group and the redox core typically prevents any interplay between π-overlap interactions and, for example, hydrogen bonding. However, direct attachment does not imply that this functionality and the TTF core are in a rigid relative disposition. Indeed, as observed here, the *ortho*-C_{TTF}–C_{amide} bonds can rotate freely in solution to afford a variety of donor conformations which may eventually be singled out in the solid state in the course of the electrocrystallization experiment. This observation, valid in the case of difunctionalized TTF derivatives, is still true in the case of monofunctionalized donors.[33]

A DFT investigation of the structural isomerism: As was seen before, a dynamic equilibrium between open and closed conformations occurs in solution for **1**–**7** on the NMR timescale, and no splitting of the single ^{1}H resonance was detected, even at a temperature as low as −90 °C. This implies a weak rotational barrier between the two amido groups, that is, a rather small stabilization energy of a closed form due to the intramolecular hydrogen bond. However, in the solid state, this stabilization, along with packing and van der Waals considerations, leads to the crystallization of closed conformers in **1**–**3** and **7**, whereas an open conformer

crystallized in the case of **4**–**6**. Moreover, the closed and open conformer are stabilized in $[\mathbf{1}]_2^{\bullet+}ReO_4$ and β''-$[\mathbf{1}]_2^{\bullet+}ClO_4$, respectively. Geometry optimizations were performed to establish which of the conformers are energy minima for both discrete neutral and oxidized donors. For this purpose we considered the simpler derivatives TTF-$(CONHMe)_2$ (**8**), its radical cation ($\mathbf{8}^{\bullet+}$), and TTF-$(CONH\mathit{n}Bu)_2$ (**9**) as model compounds for **1**, $\mathbf{1}^{\bullet+}$, and **4**, respectively. Experimental data for $\mathbf{1}^{+\bullet}$ were taken from the X-ray structure of the chloride salt, in which the donor:anion ratio is 1:1 instead of 2:1, as in the ReO_4^- and ClO_4^- salts.[34] Optimizations for **8** and $\mathbf{8}^{\bullet+}$ were done at the HF/6-31G* and B3LYP/6-31G* levels, and all frequencies were positive for the converged geometries. Selected parameters for the calculated structures and the corresponding experimental data for **1** and $\mathbf{1}^{\bullet+}$ are listed in Table 7. Both methods gave satisfactory results for the bond lengths in comparison with the experimental ones, albeit slightly longer (up to +2.5%) with DFT and randomly distributed (±2.5%) with HF calculations. As expected for this class of π-donor molecules,[35] when passing from **8** to its radical cation $\mathbf{8}^{\bullet+}$ or from **1** to [**1**]Cl, the C=C bonds lengthen, while the C–S bonds shorten, in agreement with the symmetry of the TTF core HOMO. Data in closer agreement with experiment were obtained by the DFT methodology for the N14···O15 distance defining the intramolecular hydrogen bond and the C6-C7-C11-N12 and C7-C6-C13-N14 dihedral angles, whose values are a signature of the type of conformation, (i.e, open or closed) of the *ortho*-diamide skeleton. The calculated DFT geometry for **8**, shown in Figure 16, corresponds to a closed form with an intramolecular N14–H···O15 bond. The HF calculation leads to a similar conformer. In the case of $\mathbf{8}^{\bullet+}$, the geometry optimization also converged to a closed form with both methods. The conformation within the *ortho*-diamide framework resembles that in Figure 1, and the overall geometry is very similar to that of $\mathbf{1}^{\bullet+}$ in **1**-Cl.

Thus, the closed form is a minimum for **8** and its radical cation, which is not surprising, since in the gas phase no other interaction competes with this intramolecular hydrogen bond. In the solid state, weak intermolecular interactions such as van der Waals forces, p_π–p_π interactions, and intermolecular hydrogen bonds could eventually overcome the net stabilization energy associated with the formation of an intramolecular hydrogen bond and thus favor crystallization of an open form. As noted before, this is observed in the $[\mathbf{1}]_2^{\bullet+}ClO_4$ salt. Also, a steady lengthening of the N–H···O intramolecular distance with increasing length of the hydrophobic chain is observed in the **1**–**3** series, which means a weakening of the intramolecular hydrogen bond. This bond completely breaks in the case of **4**. On the contrary, the DFT optimization at the B3LYP/6-31G* level of the geometry of **9**, not detailed further hereafter, on an input geometry derived from the X-ray structure of **4**, leads to a closed conformer as an energy minimum. Again, intermolecular interactions occurring in the solid state are likely to be responsible for the experimentally observed conformation of **4**. However, in the DFT optimized geometry of **9** the N23···O22 distance (2.746 Å) defining the intramolecular N23–H···O22 hydrogen bond is slightly longer than the corresponding N14···O15 distance (2.739 Å) in **8**. This clearly shows the tendency of this intramolecular hydrogen bond to weaken with increasing length of the hydrophobic chain. Since the experimental open conformation of **4** does not correspond to the optimized closed conformation of **9**, we performed a second DFT optimization geometry on **9**, this time by freezing in the calculation the values of the two dihedral angles defining rotation of the amido groups. In the X-ray structure of **4** these angles are C3-C2-C1-N1 and C2-C3-C4-N2, which, with values of −41.69 and −32.68°, respectively, thus define an open-type conformation. The calculation converged to a structure whose energy was only 6.25 kcal mol^{-1} higher than the energy of the fully optimized structure with the closed conformation. Such an energy difference is small

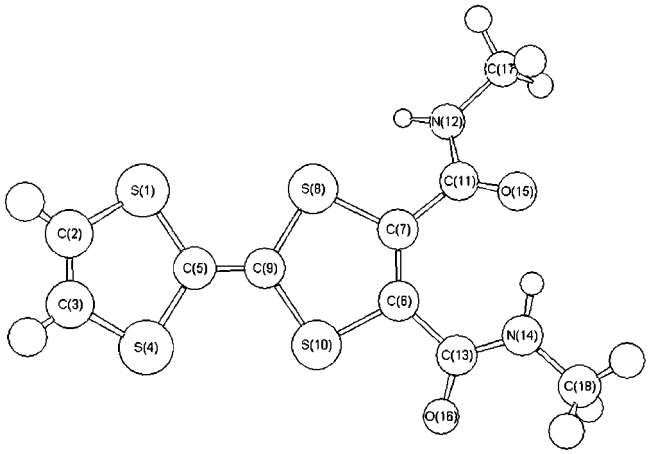

Figure 16. Calculated DFT geometry for **8**.

Table 7. Optimized geometries of **8** and $\mathbf{8}^{\bullet+}$.[a] Comparison with corresponding experimental X-ray parameters for **1** and $[\mathbf{1}]^{\bullet+}Cl^-$.

	8		**1**	$[\mathbf{1}]^{\bullet+}Cl^-$	$\mathbf{8}^{\bullet+}$	
	HF[b]	DFT[c]			HF[b,d]	DFT[c,d]
C5–C9	1.326	1.350	1.334(7)	1.363(8)	1.393	1.398
C6–C7	1.329	1.358	1.348(7)	1.352(8)	1.336	1.362
C2–C3	1.316	1.337	1.326(7)	1.358(9)	1.326	1.347
C9–S8	1.770	1.780	1.752(5)	1.729(6)	1.728	1.745
C9–S10	1.770	1.778	1.745(5)	1.715(6)	1.714	1.743
C6–S10	1.769	1.772	1.747(6)	1.742(6)	1.752	1.759
C7–S8	1.774	1.786	1.737(5)	1.744(6)	1.754	1.764
N14···O15	2.826	2.739	2.670(6)	2.707(4)	2.844	2.774
C6-C7-C11-N12	132.3	146.7	150.1	160.8	137.8	148.8
C7-C6-C13-N14	31.4	21.5	4.9	5.9	21.0	13.7

[a] Bond lengths and distances in angstroms; torsional angles in degrees. [b] Optimized geometries at the HF/6-31G* level. [c] Optimized geometries at the B3LYP/6-31G* level. [d] An unrestricted calculation was performed for the radical cation.

enough to be readily overcome by other stabilizing intermolecular interactions in the solid state. Therefore, the crystallization of **4** in an open form is not surprising with regard to the calculation result.

To assess the flexibility of the *ortho* secondary diamides, we performed DFT calculations at the B3LYP/6-31G* level to investigate the effect of the rotation of the amido groups on the energy profile of the molecule. Recent reports dealing with functional molecules containing an intramolecular hydrogen bond also focused on the calculation of torsion potentials about the groups involved in this interaction.[36,37] For example, Tsuzuki et al.[37] found an internal rotational barrier of 7.30 kcal mol^{-1} for *o*-hydroxyanisole, with an energy minimum corresponding to a planar conformation with an intramolecular O–H···OMe bond. For this study we chose bis(*N*-methyl)maleodiamide as model compound, because it appropriately mimics the fluxional part of donor **1**, namely, the two secondary amido groups in a *cis* conformation on a C=C bond, and it requires reasonable calculation time. The DFT optimization of the geometry of the molecule at the B3LYP/6-31G* level leads to a closed form in a planar conformation with an intramolecular N7–H14···O5 hydrogen bond. The dihedral angles D1 (C2-C1-C3-N4) and D2 (C1-C2-C6-N7) are 180 and 0°, respectively. Starting from this equilibrium geometry, we decreased D1 in steps of 30° in a full simulated rotation of the corresponding amido group about C1–C3. At each step of the simulation we fully optimized the geometry with respect to the D1 value. The potential energy curve and optimized geometry of the molecule are shown in Figure 17, and the D2 angles, N···O distances and relative energy values corresponding to D1 values at each scan are listed in Table 8.

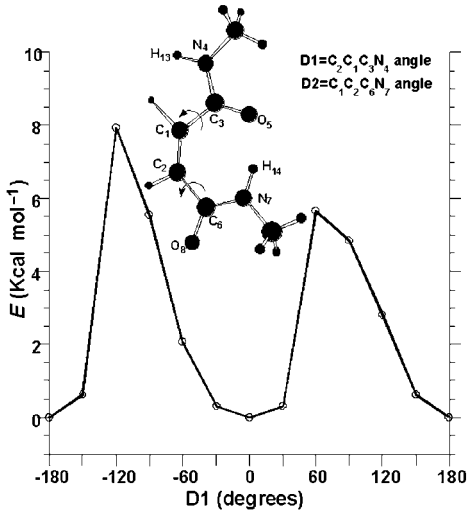

Figure 17. DFT optimized geometry of bis(*N*-methyl)maleodiamide at the B3LYP/6-31G* level.

The overall shape of the curve is symmetric, with two minima of 0 kcal mol^{-1} for D1 = 180 and 0°, and two maxima of 5.7 and 7.9 kcal mol^{-1} for D1 = 60 and −120°, respectively. The first minimum corresponds to the equilibrium starting geometry, and the second to the similar structure in which both dihedral angles are rotated by 180° and the intramolecular hydrogen bond is now N4–H13···O8. The amido groups undergo conrotatory counterclockwise movement during the simulation, which means that, apart from planar situations, the two nitrogen atoms are always situated above and below the mean plane defined by C3, C1, C2, and C6. This conrotatory rotation allows an intramolecular hydrogen bond to be preserved for as long as possible. Its breaking probably occurs somewhere between D1 = 120 and 90° in the first half of the curve, since the corresponding N7–H14···O5 distance increases from 2.864 to 3.135 Å. The same behavior is observed for the left half of the curve, with values of 2.821 Å (D1 = −60°) and 3.031 Å (D1 = −90°) for the N4–H13···O8 distance in this case. In the two optimized geometries corresponding to the energy maxima, the intramolecular hydrogen bond is clearly no longer observed, the N7(4)···O5(8) distances being greater than 3.5 Å. A sudden gain in energy, due to re-establishment of the hydrogen bond, occurs when D1 changes from 60 to 30° and from −120 to −150°. The slight difference (2.2 kcal mol^{-1}) between the two maxima is likely due to the flatness of the potential energy surface associated with the rotation of the amido groups. According to the Eyring equation[38] the coalescence temperature in the ^{1}H NMR spectrum, associated with a rotational barrier of 7.9 kcal mol^{-1}, is estimated at about −100 °C. The experimental value is likely to be even lower, since calculated energies are often overestimated compared to experimental ones. Thus, it is now obvious why we could not detect the most stable conformers by low-temperature ^{1}H NMR measurements, since this theoretical study clearly shows that the EDT-TTF-(CONHR)$_2$ series is highly flexible with respect to rotation of the amido groups.

Table 8. Parameters and relative energies for calculated PES at the DFT-B3LYP/6-31G* level of bis(*N*-methyl)maleodiamide upon stepwise variation of D1 (C2-C1-C3-N4 dihedral angle) by increments of 30°.

D1 [°]	D2[a] [°]	N···O [Å] (shortest)	ΔE [kcal mol^{-}]
180.0	0.0	2.752 (N7···O5)	0.0
150.0	23.0	2.774 (N7···O5)	0.6
120.0	32.1	2.864 (N7···O5)	2.8
90.0	37.4	3.135 (N7···O5)	4.8
60.0	56.3	3.738 (N7···O5)	5.7
30.0	167.2	2.767 (N4···O8)	0.3
0.0	180.0	2.750 (N4···O8)	0.0
−30.0	−167.2	2.767 (N4···O8)	0.3
−60.0	−159.6	2.821 (N4···O8)	2.1
−90.0	−165.4	3.031 (N4···O8)	5.5
−120.0	−160.4	3.511 (N4···O8)	7.9
−150.0	−23.1	2.774 (N7···O5)	0.6

[a] C1-C2-C6-N7 dihedral angle.

Analogy between the conformation and solid-state expression of bis(secondary *ortho*-diamide)-EDT-TTF dimers and bis(secondary *ortho*-diamide)metallocenes: Seeking to test the principle of flexibility between the closed and open conformations of conjugated secondary *ortho*-diamides in directing solid-state structures, we conducted a search of the Cambridge data base and found 1,1′,2,2′-tetrakis(*tert*-butylcarbamoyl)ferrocene and 1,1′,2,2′-tetrakis(*tert*-butylcarbamoyl)ruthenocene, two metallocenes reported recently by

Erker et al.[39] In the context of the present paper, it is especially enlightening to analyze the patterns of intermolecular interactions in their crystal structures (Figure 18). Thus, in the solid state, the two secondary *ortho*-diamide groups attached to each Cp ring of the ferrocene are in the typical closed conformation imposed by a NH···O hydrogen-bonded seven-membered ring, while the open structural isomer appears to be stabilized in the crystal structure of the ruthenocene. In the latter, as a consequence, hydrogen bonding takes place between amido groups belonging to two different Cp rings. A striking analogy can be drawn if one considers that any $[\text{EDT-TTF-(CONHMe)}_2]_2$ dimer as in $[\mathbf{1}]_2^{\cdot+}\text{ReO}_4$ or $[\mathbf{1}]_2^{\cdot+}\text{ClO}_4$ resembles a metallocene (Figure 18). The two TTF cores may rotate versus one another to form centro- or noncentrosymmetric dimers, just as the Cp rings do in the ferrocene and ruthenocene, respectively. Then, these two sets of similar pairs of conformers (Figure 18 a/b and c/d) are expressed in two different crystal structures by virtue of similar intermolecular N–H···O hydrogen bonds. Of course, the major difference between a metallocene and a $[\text{EDT-TTF-(CONHMe)}_2]_2$ dimer, namely, p_π–p_π overlap interactions, affect the balance of weak intermolecular interactions and ultimately impose different overall architectures, even though the patterns of intra- and intermolecular associations and the flexibility of the conformers are analogous. These observations call for an exploration of a phase diagram of bimolecular adducts such as $[\text{EDT-TTF-(CONHMe)}_2]_2$[1,1′,2,2′-tetrakis(*tert*-butylcarbamoyl)ferrocene]ReO_4 and $[\text{EDT-TTF-(CONHMe)}_2]_2$[1,1′,2,2′-tetrakis(*tert*-butylcarbamoyl)ruthenocene]ClO_4, with the aim of self-assembly of the former by electrocrystallization, or any combination of couples of somewhat dissimilar redox-active precursors capable of association by self-complementary hydrogen bonding.

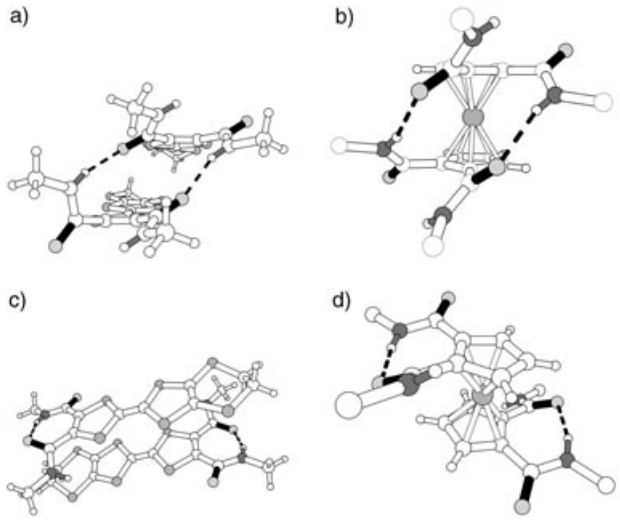

Figure 18. Illustration of the analogy of intra- and intermolecular NH···O hydrogen-bond patterns, motif conformations, and shapes between a) $[\mathbf{1}]_2^{\cdot+}$ in β″-$[\mathbf{1}]_2^{\cdot+}\text{ClO}_4$; b) 1,1′,2,2′-tetrakis(*tert*-butylcarbamoyl)ruthenocene; c) $[\mathbf{1}]_2^{\cdot+}$ in $[\mathbf{1}]_2^{\cdot+}\text{ReO}_4$; and d) 1,1′,2,2′-tetrakis(*tert*-butylcarbamoyl)ferrocene. The methyl groups of the *tert*-butylcarbamoyl moieties have been omitted for clarity.

Conclusion

The foregoing results demonstrate the ability of a π redox core functionalized with two secondary amido groups in *ortho* positions, that is, EDT-TTF-(CONHR)_2 (R = Me, **1**; Et, **2**; Pr, **3**; Bu, **4**; Pent, **5**; Hex, **6**, Bz, **7**), to be expressed into vastly different crystalline topologies which primarily differ by the occurrence or absence of an intramolecular N–H···O hydrogen bond closing a seven-membered ring. This introduces a genuine flexibility in the balance of intra- to intermolecular expression of the molecule by complementary hydrogen bonding interactions, since the seven-membered ring is not observed in solution, a result supported by theoretical calculations. Hence, within the series, the hydrogen-bond ring motif proved to be highly sensitive to crystal packing, as the decoration with increasingly larger side chains in the neutral, mono-component solids, as well as modification of the anion size in the radical cation salts, sacrifices its conformational uniqueness. Specifically, it is demonstrated that the observation of structural isomerism in the radical cation salts of $\text{EDT-TTF-(CONHMe)}_2$ is a direct manifestation in the solid state of a fine sensitivity of the constrained seven-membered ring to changes in internal chemical pressure exerted by either ReO_4^- or ClO_4^-, two anions of different volumes but otherwise identical charge and symmetry, since, despite having the same stoichiometry, the two salts have vastly different architectures, dimensionalities, electronic structures, and collective properties, a consequence of the presence of the closed or open structural isomers in one or the other. These are valuable observations in the field of crystal engineering, where the concept of synthon qualifies the duality of a functionality associated with the topology of its pattern of intermolecular association. It must be taken into account that synthons may not be rigid and the flexibility conferred on the molecule is a key parameter in the a priori prediction of crystal structures. These results demonstrate that the Coulomb energy, intermolecular p_π–p_π overlap interactions, and bandwidth of electronic molecular materials may be manipulated by creation of structural isomers of radical cation salts on tuning their internal chemical pressure.

Experimental Section

General procedure for the preparation of 1–7: A solution of $\text{EDT-TTF-(CO}_2\text{Me)}_2$[24] in CH_3CN (30 mL) (200 mg, 0.48 mmol) was treated with an excess of the appropriate amine NH_2R (Aldrich) in aqueous solution. After 24 h of stirring at room temperature, the resulting precipitate was collected by filtration and recrystallized twice.

4,5-Ethylenedithio-4′,5′-bis(methylcarbamoyl)tetrathiafulvalene (1): Dark red needles (187 mg, 94 %) recrystallized from acetonitrile, m.p. 218–219 °C; ^{1}H NMR (400 MHz, [D$_6$]DMSO): $\delta = 8.75$ (br s, 2H; NH), 3.40 (s, 4H; CH_2CH_2), 2.68 ppm (d, $^3J(\text{H,H}) = 4.5$ Hz, 6H; CH_3); ^{13}C NMR (100 MHz, [D$_6$]DMSO): $\delta = 160.04$ (C=O), 133.32 (C–CO), 113.97, 112.21, 106.92 (C=C), 30.45 (CH_2CH_2), 27.39 ppm (CH_3); IR (KBr): $\tilde{\nu}$ =

3407–3174 (N–H), 1653–1634 cm^{-1} (C=O); UV/Vis (THF): λ_{max} (ε) = 446 nm (1430 $mol^{-1}dm^3cm^{-1}$); MS (70 eV, EI): *m/z* (%): 408 (100) $[M]^+$; elemental analysis (%) calcd for $C_{12}H_{12}N_2O_2S_6$ (408.6): C 35.27, H 2.96, N 6.86; found: C 35.26, H 2.95, N 6.97.

4,5-Ethylenedithio-4′,5′-bis(ethylcarbamoyl)tetrathiafulvalene (2): Dark red needles (110 mg, 52%) recrystallized from acetonitrile, m.p. 180–181 °C; ^{1}H NMR (400 MHz, $CDCl_3$): δ = 7.98 (br s, 2H; NH), 3.34 (quint, ^3J(H,H) = 7.3 Hz, 4H; CH_2), 3.29 (s, 4H; CH_2CH_2), 1.19 ppm (t, ^3J(H,H) = 7.3 Hz, 6H; CH_3); ^{13}C NMR (100 MHz, $CDCl_3$): δ = 160.03 (C=O), 134.49 (C–CO), 114.52, 109.99, 109.21 (C=C), 35.82 (CH_2), 30.66 (CH_2CH_2), 14.70 ppm (CH_3); IR (KBr): $\tilde{\nu}$ = 3306–3221 (NH), 2969–2929 (CH_3, CH_2), 1646–1621 cm^{-1} (C=O); UV/Vis (THF): λ_{max} (ε) = 443 nm (1420 $mol^{-1}dm^3cm^{-1}$); MS (70 eV, EI): *m/z* (%): 436 (100) $[M]^+$; elemental analysis (%) calcd for $C_{14}H_{16}N_2O_2S_6$ (436.7): C 38.51, H 3.69, N 6.41; found: C 38.38, H 3.71, N 6.37.

4,5-Ethylenedithio-4′,5′-bis(propylcarbamoyl)tetrathiafulvalene (3): Red prisms (135 mg, 60%) recrystallized from acetonitrile, m.p. 150–151 °C; ^{1}H NMR (400 MHz, $CDCl_3$): δ = 8.06 (br t, ^3J(H,H) = 7.3 Hz, 2H; N–H), 3.29 (s, 4H; CH_2CH_2), 3.25 (q, ^3J(H,H) = 7.3 Hz, 4H; CH_2), 1.58 (sext, ^3J(H,H) = 7.3 Hz, 4H; CH_2), 0.96 ppm (t, ^3J(H,H) = 7.3 Hz, 6H; CH_3); ^{13}C (100 MHz, $CDCl_3$): δ = 160.44 (C=O), 134.54 (C–CO), 114.77, 110.33, 109.08 (C=C), 42.81 (CH_2), 30.86 (CH_2CH_2), 22.98 (CH_2), 12.07 ppm (CH_3); IR (KBr): $\tilde{\nu}$ = 3257 (NH), 2961, 2927, 2870 (CH_3, CH_2), 1649–1625 cm^{-1} (C=O); UV/Vis (THF): λ_{max} (ε) = 443 nm (1500 $mol^{-1}dm^3cm^{-1}$); MS (70 eV, EI): *m/z* (%): 464 (100) $[M]^+$; elemental analysis (%) calcd for $C_{16}H_{20}N_2O_2S_6$ (464.7): C 41.35, H 4.34, N 6.03; found: C 41.41, H 4.03, N 6.08.

4,5-Ethylenedithio-4′,5′-bis(butylcarbamoyl)tetrathiafulvalene (4): Red needles (175 mg, 73%) recrystallized from acetonitrile, m.p. 196–197 °C; ^{1}H NMR (400 MHz, [D$_6$]DMSO): δ = 8.84 (br t, ^3J(H,H) = 7.2 Hz, 2H; NH), 3.44 (s, 4H; CH_2CH_2), 3.17 (q, ^3J(H,H) = 7.2 Hz, 4H; CH_2), 1.45 (quint, ^3J(H,H) = 7.2 Hz, 4H; CH_2), 1.31 (sext, ^3J(H,H) = 7.2 Hz, 4H; CH_2), 0.91 ppm (t, ^3J(H,H) = 7.2 Hz, 6H; CH_3); ^{13}C NMR (100 MHz, [D$_6$]DMSO): δ = 159.63 (C=O), 133.25 (C–CO), 113.99, 112.25, 106.92 (C=C), 31.53 (CH_2), 31.44 (CH_2), 30.46 (CH_2CH_2), 20.31 (CH_2), 14.44 ppm (CH_3); IR (KBr): $\tilde{\nu}$ = 3258 (NH), 2949, 2923, 2864 (CH_3, CH_2), 1662–1623 cm^{-1} (C=O); UV/Vis (THF): λ_{max} (ε) = 443 nm (1410 $mol^{-1}dm^3cm^{-1}$); MS (70 eV, EI): *m/z* (%): 492 (100) $[M]^+$; elemental analysis (%) calcd for $C_{18}H_{24}N_2O_2S_6$ (492.8): C 43.87, H 4.91, N 5.68; found: C 43.82, H 5.04, N 5.93.

4,5-Ethylenedithio-4′,5′-bis(pentylcarbamoyl)tetrathiafulvalene (5): Red needles (140 mg, 55%) recrystallized from acetonitrile, m.p. 185–186 °C; ^{1}H NMR (500 MHz, $CDCl_3$): δ = 7.97 (br s, 2H; NH), 3.29 (s, 8H; CH_2CH_2, CH_2), 1.54 (q, ^3J(H,H) = 7 Hz, 4H; CH_2), 1.32 (m, 12H; CH_2), 0.90 ppm (t, ^3J(H,H) = 7 Hz, 6H; CH_3); MS (70 eV, EI): *m/z* (%): 520 (26) $[M]^+$; elemental analysis (%) calcd for $C_{20}H_{28}N_2O_2S_6$ (520.8): C 46.12, H 5.42, N 5.38; found: C 46.29, H 5.25, N 5.21.

4,5-Ethylenedithio-4′,5′-bis(hexylcarbamoyl)tetrathiafulvalene (6): Red platelets (190 mg, 71%) recrystallized from acetonitrile, m.p. 145–146 °C; ^{1}H NMR (400 MHz, $CDCl_3$): δ = 8.02 (br s, 2H; NH), 3.28 (s, 8H; CH_2CH_2, CH_2), 1.51 (q, ^3J(H,H) = 7 Hz, 4H; CH_2), 1.33 (m, 12H; CH_2), 0.91 ppm (t, ^3J(H,H) = 7 Hz, 6H; CH_3); IR (KBr): $\tilde{\nu}$ = 3263–3242 (NH), 2946, 2922, 2846 (CH_3, CH_2), 1660–1622 (C=O) cm^{-1}; MS (70 eV, EI): *m/z* (%): 548 (35) $[M]^+$; elemental analysis (%) calcd for $C_{22}H_{32}N_2O_2S_6$ (548.9): C 48.14, H 5.88, N 5.10; found: C 48.37, H 5.98, N 4.84.

4,5-Ethylenedithio-4′,5′-bis(benzylcarbamoyl)tetrathiafulvalene (7): Red needles (160 mg, 58%) recrystallized from toluene/acetonitrile, m.p. 180–181 °C; ^{1}H NMR (400 MHz, [D$_6$]DMSO): δ = 9.35 (t, ^3J(H,H) = 5.66 Hz, 2H; NH), 7.32 (m, 10H; CH), 4.37 (d, ^3J(H,H) = 5.66 Hz, 4H; CH_2), 3.43 ppm (s, 4H; CH_2CH_2); ^{13}C (100 MHz, [D$_6$]DMSO): δ = 159.75 (C=O), 138.95 (C_{ipso}), 133.35 (C-CO), 129.23 (C_{ortho}), 128.16 (C_{meta}), 127.90 (C_{para}), 114.02, 112.10, 107.49 (C=C), 43.95 (CH_2), 30.46 ppm (CH_2CH_2); IR (KBr): $\tilde{\nu}$ = 3264–3168 (NH), 1654–1625 (C=O), 1642 cm^{-1} (C=C); UV/Vis (THF): λ_{max} (ε) = 448 nm (1400 $mol^{-1}dm^3cm^{-1}$); MS (70 eV, EI): *m/z* (%): 560 (5) $[M]^+$, 91 (100) $[C_7H_7]^+$; elemental analysis (%) calcd for $C_{24}H_{20}N_2O_2S_6$ (560.8): C 51.40, H 3.59, N 4.99; found: C 51.11, H 3.55, N 4.82.

Cyclic voltammetry: Experiments were performed at 25 °C in THF with nBu$_4$NPF$_6$ (5×10^{-2} mol L^{-1}) as supporting electrolyte.

Electrocrystallization experiments: Compound **1** (5 mg) was oxidized in the presence of the tetra-*n*-butylammonium salt of the desired counteranion (50 mg) in freshly distilled CH_3CN (12 mL). The experiment was carried out in two-compartment cells with platinum wires (L = 2 cm, $\varnothing$ = 1 mm) at a constant current (0.5 μA) at 25 °C.[22]

X-ray data collection and structure determination: Data were collected on an Imaging Plate Diffraction System (STOE-IPDS) for **2**–**5**, **7**, and $[\mathbf{1}]_2^{\cdot+}ReO_4$, and on an Enraf-Nonius Mach 3 diffractometer for **1** and $[\mathbf{1}]_2^{\cdot+}ClO_4$. Structures were solved by direct methods using SHELXS-86 and refined byfull-matrix least-squares method on F^2 using SHELXL-93 (G. M. Sheldrick, University of Göttingen, 1993). The hydrogen atoms were introduced at calculated positions (riding model) with C–H and NH bond lengths of 0.97 and 0.86 Å, respectively. In the structures of **1**–**4** and **7**, all non-hydrogen atoms were refined with anisotropic displacement parameters. For **5**, C9, C19, and C20 were refined with isotropic parameters. In $[\mathbf{1}]_2^{\cdot+}ReO_4$ at 293 K, the ethylenedithio bridge of molecule $\mathbf{1}_A$ as well as two oxygen atoms of the ReO_4^- ion exhibited disorder and were refined isotropically. In $[\mathbf{1}]_2^{\cdot+}ClO_4$ at 293 K, one oxygen atom of the ClO_4^- ion was disordered over two positions and was refined isotropically. CCDC 229879–229887 contain the supplementary crystallographic data for this paper. These data can be obtained free of charge via www.ccdc.cam.ac.uk/conts/retrieving.html (or from the Cambridge Crystallographic Data Centre, 12 Union Road, Cambridge CB2 1EZ, UK; fax: (+44) 1223-336-033; or e-mail: deposit@ccdc.cam.ac.uk).

X-ray powder diffraction data: Crystalline powder samples of $[\mathbf{1}]_2^{\cdot+}ReO_4$ and $[\mathbf{1}]_2^{\cdot+}ClO_4$ were glued onto an oriented silicon wafer, and data were collected with a XCelerator detector operating in a scanning mode with an active length of 0.519° with monochromated $Cu_{K\alpha1}$ radiation (Ge monochromator), frontal divergence slits of 1/4° and a 20 mm mask, with a rotating sample (120 rpm) and a step size of 0.0167° in 120 s.

Band structure calculations: The tight-binding band structure calculations were based upon the effective one-electron Hamiltonian of the extended Hückel method.[40] The off-diagonal matrix elements of the Hamiltonian were calculated according to the modified Wolfsberg–Helmholz formula.[41] All valence electrons were explicitly taken into account in the calculations, and the basis set consisted of double-ζ Slater-type orbitals for C, N, O, and S, and single-ζ Slater-type orbitals for H. The exponents, contraction coefficients, and atomic parameters for C, S, and H were taken from previous work.[42] Those used for N and O were 2.261, 1.424. 0.7297, 0.3455, and −26.0 eV for N 2s; 3.249, 1.499, 0.2881, 0.7783, and −13.4 eV for N 2p; 2.688, 1.675, 0.7076, 0.3745, and −32.3 for O 2s; and 3.694, 1.658, 0.3322, 0.7448, and −14.8 eV for O 2p.

Computational details: Hartree–Fock and DFT calculations were performed with Gaussian 98[43] using the 6-31G* basis set. For DFT calculations, the B3LYP functional with a Becke gradient correction for exchange[44] and Lee–Yang–Parr corrections for correlation[45] was used.

Resistivity measurements: Resistivity measurements were performed in a liquid helium cryostat on single crystals of $[\mathbf{1}]_2^{\cdot+}ReO_4$ and $[\mathbf{1}]_2^{\cdot+}ClO_4$ by using the four-probe low-frequency lock-in technique with measuring currents ranging from 0.1 to 10 μA. To minimize the resistance of the contacts, four gold pads were evaporated along the largest face and on both sides of the plateletlike crystals. High hydrostatic pressure was provided by a clamped cell made of nonmagnetic NiCrAl alloy encapsulating a Teflon cell containing silicon oil as pressure-transmitting medium. The pressure was measured at room temperature by a small manganine gauge located in the cell next to the sample. The pressure loss arising upon cooling was neglected.

Acknowledgment

Financial support from the CNRS and the Région Pays de la Loire (PhD grant to S.A.B.) is gratefully acknowledged. We thank Dr. Philippe Pradeau, Corning SA - Centre Européen de Recherche de Fontainebleau for X-ray powder data. This work was partially supported (E.C.) by DGI-Spain (Project BFM2003-03372-C03) and Generalitat de Catalunya (Project 2001 SGR 333) and the CNRS-CSIC Program 2002-03).

[1] C. B. Aakeröy, K. R. Seddon, *Chem. Soc. Rev.* **1993**, *22*, 397.
[2] G. R. Desiraju, T. Steiner, *The Weak Hydrogen Bond*, University Press Oxford, New York, **1999**.
[3] G. A. Jeffrey, W. Saenger, *Hydrogen Bonding in Biological Structures*, Springer-Verlag, Berlin, **1991.**
[4] T. E. Creighton, *Proteins: Structure and Molecular Properties*, Freeman and Company, New York, **1993.**
[5] a) J. C. MacDonald, G. M. Whitesides, *Chem. Rev.* **1994**, *94*, 2383; b) J. C. MacDonald, G. T. R. Palmore in *The Amide Linkage: Selected Structural Aspects in Chemistry, Biochemistry and Materials Science* (Eds.: A. Greenberg, C. M. Breneman, J. F. Liebman), Wiley, New York, **2000**, pp. 291–336; c) G. R. Desiraju, *Angew. Chem.* **1995**, *107*, 2541; *Angew. Chem. Int. Ed. Engl.* **1995**, *34*, 2311.
[6] a) M. R. Bryce, *J. Mater. Chem.* **1995**, *5*, 1481;b) M. Fourmigue, P. Batail, *Chem. Rev.* **2004**, *104*, in press.
[7] K. Heuzé, M. Fourmigué, P. Batail, E. Canadell, P. Auban-Senzier, *Chem. Eur. J.* **1999**, *5*, 2971.
[8] K. Heuzé, M. Fourmigué, P. Batail, C. Coulon, R. Clérac, E. Canadell, P. Auban-Senzier, S. Ravy, D. Jérome, *Adv. Mater.* **2003**, *15*, 1251.
[9] A. J. Moore, M. R. Bryce, A. S. Batsanov, J. N. Heaton, C. W. Lehmann, J. A. K. Howard, N. Robertson, A. E. Underhill, I. F. Perepichka, *J. Mater. Chem.* **1998**, *8*, 1541.
[10] K. Heuzé, M. Fourmigué, P. Batail, *J. Mater. Chem.* **1999**, *9*, 2373.
[11] G. Ono, H. Terao, S. Higuchi, T. Sugawara, A. Izuoka, T. Mochida, *J. Mater. Chem.* **1998**, *8*, 1703.
[12] O. Neilands, S. Belyakov, V. Tilika, A. Edzina, *J. Chem. Soc. Chem. Commun.* **1995**, 325.
[13] R. P. Parg, J. D. Kilburn, M. C. Petty, C. Pearson, T. G. Ryan, *J. Mater. Chem.* **1995**, *5*, 1609.
[14] K. Heuzé, C. Mézière, M. Fourmigué, P. Batail, C. Coulon, E. Canadell, P. Auban-Senzier, D. Jérome, *Chem. Mater.* **2000**, *12*, 1898.
[15] D. M. Rudkevich, *Chem. Eur. J.* **2000**, *6*, 2679.
[16] P. Gilli, V. Bertolasi, V. Ferretti, G. Gilli, *J. Am. Chem. Soc.* **2000**, *122*, 10405.
[17] S. A. Baudron, P. Batail, C. Rovira, E. Canadell, R. Clérac, *Chem. Commun.* **2003**, 1820.
[18] M. Gray, A. O. Cuello, G. Cooke, V. M. Rotello, *J. Am. Chem. Soc.* **2003**, *125*, 7882.
[19] C. Bilton, F. H. Allen, G. P. Shields, J. A. K. Howard, *Acta Crystallogr. Sect. B* **2000**, *56*, 849.
[20] T. R. Furlani, J. F. Garvey, *Mol. Phys.* **1997**, *92*, 449.
[21] D. Missopolinou, C. Panayiotou, *J. Phys. Chem. A* **1998**, *102*, 3574.
[22] P. Batail, K. Boubekeur, M. Fourmigué, J.-C. P. Gabriel, *Chem. Mater.* **1998**, *10*, 3005.
[23] S. A. Baudron, N. Avarvari, P. Batail, C. Coulon, R. Clérac, E. Canadell, P. Auban-Senzier, *J. Am. Chem. Soc.* **2003**, *125*, 11583.
[24] P. Blanchard, M. Sallé, G. Duguay, M. Jubault, A. Gorgues, *Tetrahedron Lett.* **1998**, *39*, 2685.
[25] A. S. Batsanov, M. R. Bryce, J. N. Heaton, A. J. Moore, P. J. Skabara, J. A. K. Howard, E. Orti, P. M. Viruela, R. Viruela, *J. Mater. Chem.* **1995**, *5*, 1689.
[26] Preliminary structural information (triclinic, space group $P\bar{1}$, $a=$ 8.2496(8), $b=9.3553(8)$, $c=39.1280(40)$ Å, $\alpha=87.524(1)$, $\beta=$ 107.058(12), $\gamma=63.784(10)°$, $V=2694.5(1)$ Å^3) on **6** indicates that it adopts the same organization as **4** and **5**.
[27] M. D. Hollingsworth, M. E. Brown, B. D. Santarsiero, J. C. Huffman, C. R. Gross, *Chem. Mater.* **1994**, *6*, 1227.
[28] M. Etter, *Acc. Chem. Res.* **1990**, *23*, 120.
[29] A. T. Hagler, L. Leiserowitz, *J. Am. Chem. Soc.* **1978**, *100*, 5879.
[30] T. Mori, *Bull. Chem. Soc. Jpn.* **1998**, *71*, 2509.
[31] A. Deluzet, R. Rousseau, C. Guilbaud, I. Granger, K. Boubekeur, P. Batail, E. Canadell, P. Auban-Senzier, D. Jérome, *Chem. Eur. J.* **2002**, *8*, 3884.
[32] a) P. Batail, L. Ouahab, *Mol. Cryst. Liq. Cryst.* **1985**, *125*, 205; b) J. M. Williams, J. R. Ferraro, R. J. Thorn, K. D. Carlson, U. Geiser, H. H. Wang, A. M. Kini, M.-H. Whangbo in *Organic Superconductors (Including Fullerenes): Synthesis, Structure, Properties and Theory* (Ed.: R. N. Grimes), Prentice Hall, Englewood Cliffs, **1992**, p. 47.
[33] In $[EDT\text{-}TTF\text{-}CO_2Me]_6[Re_6Se_8(CN)_6](CH_2Cl_2)_2$, the ester group adopts a *trans* orientation with respect to the TTF core, while it is in a *cis* orientation in $[EDT\text{-}TTF\text{-}CO_2Me]_4[Re_6S_8(CN)_6](CH_3CN)_2$: S. A. Baudron, O. J. Dautel, P. Batail, unpublished results.
[34] Crystal data for **1**-Cl at 200 K: monoclinic, space group *I*2/*a*, $a=$ 9.5894(9), $b=25.864(2)$, $c=14.4042(16)$ Å, $\beta=107.058(12)°$, $V=$ 3415.4(6) Å^3. Unpublished results.
[35] P. Guionneau, C. J. Kepert, G. Bravic, D. Chasseau, M. R. Truter, M. Kurmoo, P. Day, *Synth. Met.* **1997**, *86*, 1973.
[36] I. C. L. Barros, C. C. C. Bejan, J. B. P. da Silva, F. W. J. Demnitz, F. Hallwass, H. U. Gremlich, *J. Org. Chem.* **2002**, *67*, 370.
[37] S. Tsuzuki, H. Houjou, Y. Nagawa, K. Hiratani, *J. Phys. Chem. A* **2000**, *104*, 1332.
[38] H. Eyring, *Chem. Rev.* **1935**, *35*, 65.
[39] K. Klaß, R. Fröhlich, G. Erker, *J. Chem. Soc. Dalton Trans.* **1999**, 4457.
[40] M.-H. Whangbo, R. Hoffmann, *J. Am. Chem. Soc.* **1978**, *100*, 6093.
[41] J. H. Ammeter, H.-B. Bürgi, J. Thibeault, R. Hoffmann, *J. Am. Chem. Soc.* **1978**, *100*, 3686.
[42] A. Pénicaud, K. Boubekeur, P. Batail, E. Canadell, P. Auban-Senzier, D. Jérome, *J. Am. Chem. Soc.* **1993**, *115*, 4101.
[43] Gaussian 98, Revision A.7, M. J. Frisch, G. W. Trucks, H. B. Schlegel, G. E. Scuseria, M. A. Robb, J. R. Cheeseman, V. G. Zakrzewski, J. A. Montgomery, Jr., R. E. Stratmann, J. C. Burant, S. Dapprich, J. M. Millam, A. D. Daniels, K. N. Kudin, M. C. Strain, O. Farkas, J. Tomasi, V. Barone, M. Cossi, R. Cammi, B. Mennucci, C. Pomelli, C. Adamo, S. Clifford, J. Ochterski, G. A. Petersson, P. Y. Ayala, Q. Cui, K. Morokuma, D. K. Malick, A. D. Rabuck, K. Raghavachari, J. B. Foresman, J. Cioslowski, J. V. Ortiz, A. G. Baboul, B. B. Stefanov, G. Liu, A. Liashenko, P. Piskorz, I. Komaromi, R. Gomperts, R. L. Martin, D. J. Fox, T. Keith, M. A. Al-Laham, C. Y. Peng, A. Nanayakkara, C. Gonzalez, M. Challacombe, P. M. W. Gill, B. Johnson, W. Chen, M. W. Wong, J. L. Andres, C. Gonzalez, M. Head-Gordon, E. S. Replogle, and J. A. Pople, Gaussian, Inc., Pittsburgh PA, **1998**.
[44] a) A. D. Becke, *Phys. Rev. B* **1986**, *33*, 8822; A. D. Becke, *ACS Symp. Ser.* **1989**, *394*, 165; b) A. D. Becke, *Int. J. Quantum Chem.* **1989**, Symp. no. *23*, 599.
[45] C. Lee, W. Yang, R. G. Parr, *Phys. Rev. B* **1988**, *41*, 785.
[46] O. J. Dautel, M. Fourmigué, *J. Org. Chem.* **2000**, *65*, 6479.
[47] H. Oku, N. Ueyama, A. Nakamura, *Inorg. Chem.* **1997**, *36*, 1504.
[48] F. H. Allen, C. M. Bird, R. S. Scott, P. R. Raithby, *Acta Crystallogr. Sect. B* **1997**, *53*, 696.
[49] W. D. S. Motherwell, G. P. Shields, F. H. Allen, *Acta Crystallogr. Sect. B* **2000**, *56*, 857.
[50] L. Leiserowitz, M. Tuval, *Acta Crystallogr. Sect. B* **1978**, *34*, 1230.
[51] R. Taylor, O. Kennard, W. Versichel, *Acta Crystallogr. Sect. B* **1984**, *40*, 280.

Received: February 16, 2004
Published online: July 27, 2004

